

Spin and parity measurement of the $\Lambda(1405)$ baryon

K. Moriya,^{1,*} R.A. Schumacher,^{1,†} M. Aghasyan,¹⁶ M.J. Amarian,²⁷ M.D. Anderson,³⁴ S. Anefalos Pereira,¹⁶ J. Ball,⁷ N.A. Baltzell,^{2,31} M. Battaglieri,¹⁷ M. Bellis,^{1,‡} A.S. Biselli,¹⁰ J. Bono,¹¹ S. Boiarinov,³² W.J. Briscoe,¹³ W.K. Brooks,^{33,32} V.D. Burkert,³² D.S. Carman,³² A. Celentano,¹⁷ S. Chandavar,²⁶ G. Charles,¹⁹ P.L. Cole,¹⁴ P. Collins,⁶ M. Contalbrigo,¹⁵ O. Cortes,¹⁴ V. Crede,¹² A. D'Angelo,^{18,29} N. Dashyan,³⁷ R. De Vita,¹⁷ E. De Sanctis,¹⁶ B. Dey,¹ C. Djalali,³¹ M. Dugger,³ R. Dupré,¹⁹ H. Egiyan,³² A. El Alaoui,^{33,2} L. El Fassi,² L. Elouadrhiri,³² P. Eugenio,¹² G. Fedotov,^{31,30} S. Fegan,¹⁷ J.A. Fleming,⁹ G.P. Gilfoyle,²⁸ K.L. Giovanetti,²¹ F.X. Girod,^{32,7} W. Gohn,⁸ E. Golovatch,³⁰ R.W. Gothe,³¹ M. Guidal,¹⁹ K.A. Griffioen,³⁶ K. Hafidi,² H. Hakobyan,^{33,37} K. Hicks,²⁶ M. Holtrop,²⁴ Y. Ilieva,^{31,13} D.G. Ireland,³⁴ B.S. Ishkhanov,³⁰ E.L. Isupov,³⁰ H.S. Jo,¹⁹ K. Joo,⁸ D. Keller,³⁵ M. Khandaker,²⁵ W. Kim,²² S. Koirala,²⁷ V. Kubarovsky,³² S.V. Kuleshov,^{33,20} P. Lenisa,¹⁶ H.Y. Lu,³¹ I.J.D. MacGregor,³⁴ N. Markov,⁸ M. McCracken,^{1,§} B. McKinnon,³⁴ M.D. Mestayer,³² C.A. Meyer,¹ M. Mirazita,¹⁶ V. Mokeev,^{32,30} R.A. Montgomery,³⁴ H. Moutarde,⁷ E. Munevar,³² P. Nadel-Turonski,³² S. Niccolai,¹⁹ I. Niculescu,²¹ M. Osipenko,¹⁷ L.L. Pappalardo,¹⁵ E. Pasyuk,³² P. Peng,³⁵ J.J. Phillips,³⁴ S. Pisano,¹⁶ O. Pogorelko,²⁰ S. Pozdniakov,²⁰ J.W. Price,⁴ S. Procureur,⁷ A.J.R. Puckett,⁸ B.A. Raue,^{11,32} D. Rimal,¹¹ M. Ripani,¹⁷ B.G. Ritchie,³ A. Rizzo,¹⁸ G. Rosner,³⁴ P. Roy,¹² F. Sabatié,⁷ C. Salgado,²⁵ D. Schott,¹³ E. Seder,⁸ I. Senderovich,³ E.S. Smith,³² D. Sokhan,³⁴ G.D. Smith,³⁴ S. Stepanyan,³² S. Strauch,^{31,13} W. Tang,²⁶ H. Voskanyan,³⁷ E. Voutier,²³ N.K. Walford,⁶ D.P. Watts,⁹ L.B. Weinstein,²⁷ M. Williams,^{1,¶} M.H. Wood,⁵ N. Zachariou,³¹ L. Zana,^{9,24} J. Zhang,³² V. Ziegler,³² Z.W. Zhao,³⁵ and I. Zonta^{29,18}

(CLAS Collaboration)

¹Carnegie Mellon University, Pittsburgh, Pennsylvania 15213, USA

²Argonne National Laboratory, Argonne, Illinois 60439, USA

³Arizona State University, Tempe, Arizona 85287, USA

⁴California State University, Dominguez Hills, Carson, CA 90747, USA

⁵Canisius College, Buffalo, NY 14208, USA

⁶Catholic University of America, Washington, D.C. 20064, USA

⁷CEA, Centre de Saclay, Irfu/Service de Physique Nucléaire, 91191 Gif-sur-Yvette, France

⁸University of Connecticut, Storrs, Connecticut 06269, USA

⁹Edinburgh University, Edinburgh EH9 3JZ, United Kingdom

¹⁰Fairfield University, Fairfield CT 06824, USA

¹¹Florida International University, Miami, Florida 33199, USA

¹²Florida State University, Tallahassee, Florida 32306, USA

¹³The George Washington University, Washington, DC 20052, USA

¹⁴Idaho State University, Pocatello, Idaho 83209, USA

¹⁵INFN, Sezione di Ferrara, 44100 Ferrara, Italy

¹⁶INFN, Laboratori Nazionali di Frascati, 00044 Frascati, Italy

¹⁷INFN, Sezione di Genova, 16146 Genova, Italy

¹⁸INFN, Sezione di Roma Tor Vergata, 00133 Rome, Italy

¹⁹Institut de Physique Nucléaire ORSAY, Orsay, France

²⁰Institute of Theoretical and Experimental Physics, Moscow, 117259, Russia

²¹James Madison University, Harrisonburg, Virginia 22807, USA

²²Kyungpook National University, Daegu 702-701, Republic of Korea

²³LPSC, Université Joseph Fourier, CNRS/IN2P3, INPG, Grenoble, France

²⁴University of New Hampshire, Durham, New Hampshire 03824, USA

²⁵Norfolk State University, Norfolk, Virginia 23504, USA

²⁶Ohio University, Athens, Ohio 45701, USA

²⁷Old Dominion University, Norfolk, Virginia 23529, USA

²⁸University of Richmond, Richmond, Virginia 23173, USA

²⁹Università di Roma Tor Vergata, 00133 Rome, Italy

³⁰Skobeltsyn Nuclear Physics Institute at Moscow State University, 119899 Moscow, Russia

³¹University of South Carolina, Columbia, South Carolina 29208, USA

³²Thomas Jefferson National Accelerator Facility, Newport News, Virginia 23606, USA

³³Universidad Técnica Federico Santa María, Casilla 110-V Valparaíso, Chile

³⁴University of Glasgow, Glasgow G12 8QQ, United Kingdom

³⁵University of Virginia, Charlottesville, Virginia 22901, USA

³⁶College of William and Mary, Williamsburg, Virginia 23187, USA

³⁷Yerevan Physics Institute, 375036 Yerevan, Armenia

(Dated: February 12, 2014)

A determination of the spin and parity of the $\Lambda(1405)$ is presented using photoproduction data from the CLAS detector at Jefferson Lab. The reaction $\gamma + p \rightarrow K^+ + \Lambda(1405)$ is analyzed in the decay channel $\Lambda(1405) \rightarrow \Sigma^+ + \pi^-$, where the decay distribution to $\Sigma^+\pi^-$ and the variation of the Σ^+ polarization with respect to the $\Lambda(1405)$ polarization direction determines the parity. The $\Lambda(1405)$ is produced, in the energy range $2.55 < W < 2.85$ GeV and for $0.6 < \cos\theta_{K^+}^{\text{c.m.}} < 0.9$, with polarization $P = 0.45 \pm 0.02(\text{stat}) \pm 0.07(\text{syst})$. The analysis shows that the decays are in S wave, with the Σ^+ polarized such that the $\Lambda(1405)$ has spin-parity $J^P = \frac{1}{2}^-$, as expected by most theories.

PACS numbers: 13.30.Eg 13.60.Rj 14.20.Jn

The $\Lambda(1405)$ has long been a peculiar state in the spectrum of excited hyperons. Lying just below the $N\bar{K}$ threshold, there is no universal agreement on the nature of this state. The constituent quark model for P -wave baryons [1], which has had success in describing the nonstrange low-mass baryons, has difficulty in computing the correct mass. More recently, the chiral unitary approach [2] describes the $\Lambda(1405)$ as a dynamically generated state of two overlapping isospin-zero poles in the rescattering of the octet meson and baryon states that couple to it. Another theory describes the state as a quasisubbound state of $N\bar{K}$ embedded in a $\Sigma\pi$ continuum [3].

In all of the above theories, a crucial assumption is that the $\Lambda(1405)$ has spin-parity $J^P = \frac{1}{2}^-$. This assumption is somewhat justified by the proximity of the $\Lambda(1405)$ mass to the $\Sigma\pi$ and $N\bar{K}$ thresholds and also by previous experimental analyses which saw a rapid fall in intensity of the $\Lambda(1405)$ line shape as it crossed the $N\bar{K}$ threshold [4, 5]. Only a state that couples to $\Sigma\pi$ and $N\bar{K}$ in S wave would show such behavior, and currently, this is, in the words of Dalitz in the 1998 PDG review article, the “sole direct evidence that $J^P = \frac{1}{2}^-$ ” [6]. There is at least one model [7] that postulates the $\Lambda(1405)$ to be a $\frac{1}{2}^+$ state with P -wave coupling to the $\Sigma\pi$ final state.

While many in the field would not doubt the assertion that the $\Lambda(1405)$ has $J^P = \frac{1}{2}^-$ it is, nevertheless, important to have experimental confirmation. Previous experiments [4, 5, 8] showed that the spin was consistent with $\frac{1}{2}$, but insufficient statistics and lack of polarization of the $\Lambda(1405)$ made the parity determination impossible. Recently, the results of a photoproduction experiment by the CLAS Collaboration at the Thomas Jefferson National Accelerator Facility (Jefferson Lab) were presented [9, 10]. The exclusive reaction $\gamma + p \rightarrow K^+ + \Lambda(1405)$ was produced using an unpolarized beam and target and analyzed for the three $\Sigma\pi$ decay channels. A rapid falloff of the line shapes was seen near the $N\bar{K}$ threshold, and fits were made to the line shapes assuming an S -wave coupling to the $\Sigma\pi$ and $N\bar{K}$ final states [9, 11].

Consider an excited hyperon Y^* of spin-parity J^P that decays strongly into $Y\pi$, where Y is a ground state hyperon. The $Y\pi$ angular distribution is determined solely by J and not P . This can be shown by using the statistical tensors given by Byers and Fenster [12], where the

Y^* spin density matrix is parametrized by parameters t_L^M with $0 \leq L \leq 2J$ and $|M| \leq L$. For a state that decays strongly, the decay distribution to $Y\pi$ depends only on a subset of these parameters with L even. Furthermore, the t_L^M with M odd vanish if one picks the spin quantization axis, \hat{z} , out of the production plane. Our coordinate system is set up so that in the Y^* rest frame and in the center-of-mass (c.m.) frame for $\gamma + p \rightarrow K^+ + \Lambda(1405)$, the incoming photon direction is in the negative y direction. The direction out of the production plane is defined by $\hat{z} = \vec{p}_\gamma \times \vec{p}_{K^+} / |\vec{p}_\gamma \times \vec{p}_{K^+}|$, where \vec{p}_γ and \vec{p}_{K^+} are the momenta of the incoming photon and outgoing K^+ , respectively. For the case of spin $\frac{1}{2}$, one finds that there are no remaining degrees of freedom in the decay distribution, so it is always isotropic. For spin $\frac{3}{2}$, the decay distribution is given by

$$I(\theta_Y) \propto 1 + \frac{3(1-2p)}{2p+1} \cos^2 \theta_Y, \quad (1)$$

where θ_Y is the polar angle of the decay direction of Y in the Y^* rest frame. The parameter p describes the Y^* fraction with spin projections along the z axis with $\pm\frac{3}{2}$ and not $\pm\frac{1}{2}$ and is related to t_2^0 . In general, a higher degree of complexity in the decay distribution signals a higher minimum spin that the state may possess, but an arbitrarily high spin state may still mimic the simpler behavior of a lower spin state. In the limit of completely unpolarized Y^* production, the decay distribution will be isotropic, and no information on the spin of the state is obtainable. Conversely, this would mean that there is no positive evidence that a state has spin $\frac{1}{2}$, since it could just be a higher spin state that was produced unpolarized. Therefore, a fit to the decay distribution that is consistent with isotropy is the best possible evidence of spin $\frac{1}{2}$, but in general, this does not rule out higher spins.

With the state's spin determined, the polarization that is transferred from Y^* to Y , called \vec{Q} in Fig. 1, is related to the odd- L t_L^M . One finds that the longitudinal polarization of Y along \hat{q} , the decay direction in the Y^* rest frame, will be independent of the parity of Y^* , while the transverse polarization will change sign depending on the parity. Since the parity of the Y^* is determined by the orbital angular momentum L of the decay $Y^* \rightarrow Y\pi$, and since a measurement of \vec{Q} determines L , the parity can be found.

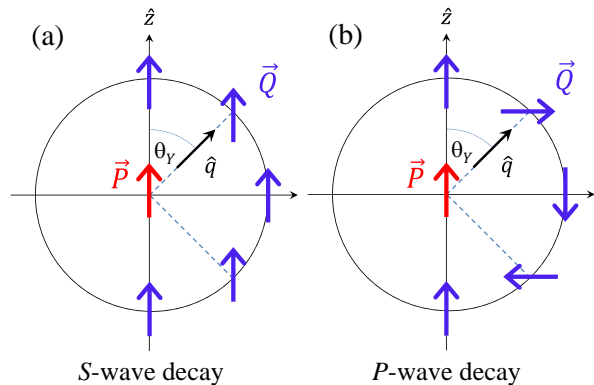


FIG. 1. (Color online) Polarization transfer from Y^* to Y in the decay $Y^* \rightarrow Y + \pi$, where Y^* has spin $\frac{1}{2}$. The red arrow shows the polarization P of the Y^* taken to be in the z direction, while the blue arrows show the polarization \vec{Q} of Y depending on the decay angle θ_Y around the z axis. (a) is for odd parity; (b) is for even parity.

A schematic of two polarization transfer scenarios depending on the parity of the Y^* is shown in Fig. 1. In the case of spin $\frac{1}{2}$, the use of an unpolarized beam and target restricts the polarization of the Y^* to be in the direction out of the production plane specified by $\vec{P} = P\hat{z}$ in Fig. 1. It can be shown that for an S -wave decay ($J^P = \frac{1}{2}^-$) of $Y^* \rightarrow Y\pi$, \vec{Q} is independent of θ_Y and is given as $\vec{Q} = \vec{P}$; that is, it retains the same polarization as that for the Y^* , so that $Q_z = P$. For a P -wave decay ($J^P = \frac{1}{2}^+$), it is given by

$$\vec{Q} = -\vec{P} + 2(\vec{P} \cdot \hat{q})\hat{q}, \quad (2)$$

so that although the magnitude is unchanged, the direction depends on \hat{q} . If a component measurement is made of the polarization along the original Y^* polarization direction, then $Q_z = P(2\cos^2\theta_Y - 1)$ so that at $\cos\theta_Y = 0$, Q_z must have the opposite sign compared to $\cos\theta_Y = \pm 1$.

In all cases, the polarization of a ground state hyperon can be measured by the weak decay asymmetry in its decay distribution into a nucleon and pion. Therefore, by measuring the polarization of the Y for different decay directions in the Y^* rest frame, we can deduce the parity of the Y^* . This method requires that the original Y^* be produced polarized, but beyond that, there are no further assumptions necessary to uniquely determine the spin and parity.

The setup of the CLAS experimental run g11a used in this analysis has been explained in Ref. [9], and further details are also available [13]. Based on the results of our previous analyses [9, 10], we select kinematic ranges where the $\Lambda(1405)$ is the dominant contribution in the $\Sigma\pi$ mass range of interest. The nine bins of energy and angle we select have c.m. energies W centered at 2.6, 2.7, and 2.8 GeV, and for each energy bin, the three forwardmost

kaon angle bins were used. The detected particles were K^+ , p , and π^- , with a kinematic fit applied to select events with a missing π^0 .

Figure 2(a) shows the $\Sigma^+\pi^-$ invariant mass $M(\Sigma^+\pi^-)$ for these nine bins combined, where the $\Lambda(1405)$ and $\Lambda(1520)$ are seen, along with background contributions from $K^+\Sigma^0(1385)$ and $K^{*0}\Sigma^+$ production. In the present analysis the backgrounds could not be removed event by event. Events were selected based on the $\Sigma^+\pi^-$ invariant mass range of 1.30–1.45 GeV/c^2 , where the spectrum is dominated by the $\Lambda(1405)$. Backgrounds due to non- $\Lambda(1405)$ production were estimated in previous works, where beside the channels listed above, a $Y^*(1670)$ background was used to parametrize the higher-mass data. We estimate these backgrounds as approximately 16% total, mostly from the $\Sigma^0(1385)$.

Figure 2(b) shows a Dalitz-like plot of the $\Sigma^+\pi^-$ invariant mass $M(\Sigma^+\pi^-)$ versus the mass $M(K^+\pi^-)$, where a slight overlap of the $K^{*0}\Sigma^+$ events (vertical band) with the $\Lambda(1405)$ and $\Lambda(1520)$ events (horizontal bands) is seen. Due to the kinematics of the reaction, the overlap is not significant and has little influence in these kinematic bins.

For each of the nine bins of W and kaon angle, each spin-parity hypothesis was tested with maximum likelihood fits to the data using a MC simulation of the data that was matched to have the same $\Sigma^+\pi^-$ invariant mass distribution as the data but generated without any angular correlations. The fit functions used joint probability distributions of the $\Sigma^+\pi^-$ angular decay distribution and the $p\pi^0$ weak decay distribution. The $\Sigma^+\pi^-$ distribution was isotropic for spin $\frac{1}{2}$ and as given in Eq. (1) for spin $\frac{3}{2}$. The $p\pi^0$ weak decay distribution used $I(\theta_p) \propto 1 + \alpha_0 Q_z \cos\theta_p$, with the polarization Q_z as a fit parameter, and θ_p is the proton decay angle in the Σ^+ rest frame. Figure 3 shows sample distributions of data and MC events for $\cos\theta_{\Sigma^+}$ (our specific $\cos\theta_Y$) and $\cos\theta_p$. The nonflatness of the $\cos\theta_{\Sigma^+}$ distribution reflects the CLAS acceptance, which varies significantly depending not only on $\cos\theta_{\Sigma^+}$ and $\cos\theta_p$ but also the azimuthal angles for each distribution. We see from Fig. 3 that the unweighted MC that was generated with isotropic distributions is able to reproduce the data well for the $\cos\theta_{\Sigma^+}$ distribution, lending support to the spin $\frac{1}{2}$ hypothesis. However, the $\cos\theta_p$ distribution requires a reweighting of MC events with a polarization to match the data, and it is this polarization of the data that allows a strong discrimination among the different hypotheses.

The $\frac{3}{2}^\pm$ hypotheses were tested but showed no significant deviation from an isotropic $\Sigma^+\pi^-$ decay distribution, and the parameter p given in Eq. (1) was seen to be consistent with $\frac{1}{2}$ (unpolarized). For each separate hypothesis, each of the MC events was assigned a weight according to its fitted intensity. The resulting distribution was compared with the data to calculate a χ^2 probability. The χ^2 probability calculated for the $\cos\theta_p$ dis-

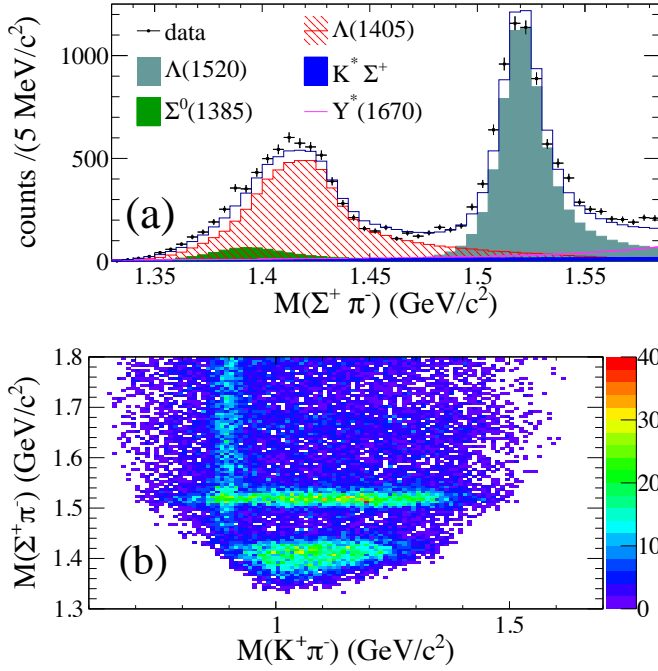


FIG. 2. (Color online) (a) $M(\Sigma^+\pi^-)$ distribution summed over the range of W and kaon angle used in this analysis. The $\Lambda(1405)$ (hatched red histogram) and $\Lambda(1520)$ (filled cyan histogram) are seen. The estimate for the main background due to the $\Sigma^0(1385)$ is superimposed (filled green area) near the bottom. Contributions from the $K^{*0}\Sigma^+$ (filled blue histogram) and $Y^*(1670)$ background (solid magenta curve) are also shown but contribute very little. The fit total is shown as the open blue histogram. (b) $M(\Sigma^+\pi^-)$ versus $M(K^+\pi^-)$ for the range of W and kaon angles used in the analysis. The vertical band is due to K^* production, while the horizontal bands show the $\Lambda(1405)$ below and the $\Lambda(1520)$ above.

tribution had the most discriminating power, and the $\frac{1}{2}^-$ case consistently had the best χ^2 probability. In our nine independent kinematic bins, the $\frac{1}{2}^+$ and $\frac{3}{2}^-$ hypotheses are typically ruled out by 3σ or more from the χ^2 probabilities and can be excluded. The three parameters describing the $\frac{3}{2}^+$ hypothesis can conspire to exactly mimic the behavior of a $\frac{1}{2}^-$ state, so definitive exclusion based on statistical tests is impossible. Fits to the $\frac{3}{2}^+$ hypothesis had worse χ^2 probabilities in all energy bins, but we also excluded it by assuming the simpler hypothesis with fewer parameters is correct.

For the cases of spin-parity $\frac{1}{2}^\pm$, the two distinct behaviors of the transferred polarization allow a simple visual illustration. Independent fits were performed in separate bins of $\cos\theta_{\Sigma^+}$. An example of the polarization Q_z in the \hat{z} direction for one bin of W and angle is shown in Fig. 4. As a function of $\cos\theta_{\Sigma^+}$, the polarization clearly does not change sign between the extremes of $\cos\theta_{\Sigma^+} = \pm 1$ and $\cos\theta_{\Sigma^+} = 0$, as would be expected from Eq. (2). We can compute the probability of each hypothesis and while the $\frac{1}{2}^-$ hypothesis consistently gives a good χ^2 probability,

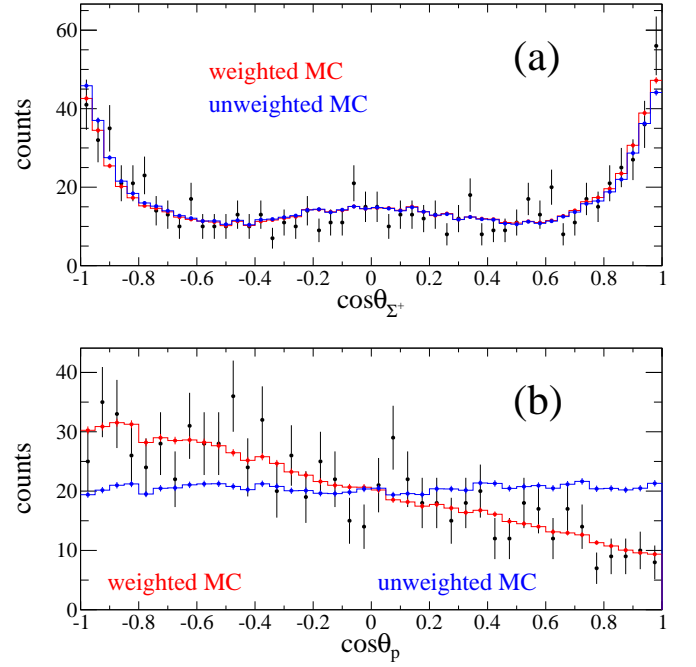


FIG. 3. (Color online) Distributions of the projections of (a) $\cos\theta_{\Sigma^+}$ and (b) $\cos\theta_p$ for $2.65 < W < 2.75$ GeV and $0.70 < \cos\theta_{K^+}^{c.m.} < 0.80$. The black points are data, the blue histograms with points are the initial MC events without weighting, and the red histograms are the MC events weighted with the fit results using the $\frac{1}{2}^-$ hypothesis. Each of the MC histograms have been scaled to have the same area as the corresponding data histograms.

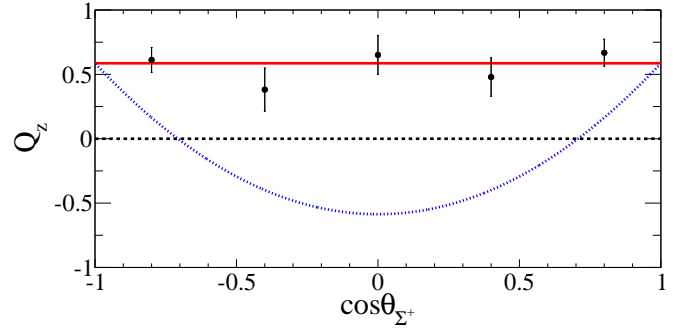


FIG. 4. (Color online) Polarization Q_z of Σ^+ versus $\cos\theta_{\Sigma^+}$ for $2.65 < W < 2.75$ GeV and $0.70 < \cos\theta_{K^+}^{c.m.} < 0.80$. The average is shown as the red solid line. The dotted blue curve is the expectation for P -wave decay.

the $\frac{1}{2}^+$ hypothesis is ruled out in its most favorable bin by at least 3.6σ and is typically ruled out by more than 5σ . With nine independent W and angle bins, the $\frac{1}{2}^+$ hypothesis is overwhelmingly ruled out.

The Σ^+ polarizations using all events in each kinematic bin with the $\frac{1}{2}^-$ hypothesis are shown in Table I. Since in this situation the polarization that is measured through the Σ^+ is equivalent to the polarization of the $\Lambda(1405)$ itself, the Q_z values in Table I represent measurements

of the $\Lambda(1405)$ polarization.

To ensure that the polarization we observe is not affected by the $\Sigma^0(1385)$, the range of $\Sigma^+\pi^-$ invariant mass was changed to reduce this contribution. With a range of 1.40–1.48 GeV/ c^2 , we estimate the contribution of the $\Sigma^0(1385)$ as 6%, and a change in polarization of 0.06 was observed. Removal of events with the $K^+\pi^-$ invariant mass within $\pm 1\Gamma$ of the K^{*0} , where Γ is the full width of the K^{*0} , gave a change of 0.02 in the final result.

As a final check that the CLAS detector is able to measure decay distributions without bias using this method, the polarization components along the x and y directions were measured. If the $\Lambda(1405)$ is a state of $\frac{1}{2}^-$, then the polarization components in the production plane should be zero. Table I shows that the measured components Q_x and Q_y are mostly consistent with zero within the statistical errors. Using these fits to estimate the systematic uncertainty of the analysis in measuring these polarizations accurately, we take ± 0.03 as an upper limit for this systematic uncertainty. We add the upper limit polarization components in the x and y directions, the uncertainty due to varying the $\Sigma^+\pi^-$ mass range, and the uncertainty due to the K^{*0} removal in quadrature to obtain the final systematic uncertainty of ± 0.07 .

To summarize, our analysis indicates that the spin-parity of the $\Lambda(1405)$ is fully consistent with $J^P = \frac{1}{2}^-$, while the $\frac{1}{2}^+$ and $\frac{3}{2}^-$ combinations are strongly disfavored. The $\frac{3}{2}^+$ combination cannot, in principle, be ruled out by statistical tests, but it did not lead to better fits, and so it is rejected. The decay angular distribution is consistent with isotropy, which strongly favors spin $\frac{1}{2}$, and under this assumption, a direct measurement of the parity has been carried out for the first time. The data strongly indicate negative parity, due to the unchanging direction of the daughter Σ^+ polarization with respect to the $\Lambda(1405)$ polarization direction. Thus, this first complete experimental test of the $\frac{1}{2}^-$ hypothesis confirms most long-held expectations. As an additional outcome, the polarization of the $\Lambda(1405)$ in photoproduction has been measured to be $0.45 \pm 0.02(\text{stat}) \pm 0.07(\text{syst})$ in the forward kaon angle region for $2.55 < W < 2.85$ GeV.

We thank Professor R. Kraemer for helpful early discussions. We acknowledge the outstanding efforts of the staff of the Accelerator and Physics Divisions at Jeffer-

son Lab that made this experiment possible. The work of the Medium Energy Physics group at Carnegie Mellon University was supported by DOE Grant No. DE-FG02-87ER40315. The Southeastern Universities Research Association (SURA) operated the Thomas Jefferson National Accelerator Facility for the United States Department of Energy under Contract No. DE-AC05-84ER40150. Further support was provided by the National Science Foundation, the United Kingdom's Science and Technology Facilities Council, and the Italian Istituto Nazionale di Fisica Nucleare.

* Current address: Indiana University, Bloomington, Indiana 47405, USA

† Contact: schumacher@cmu.edu

‡ Current address: Siena College, Loudonville, NY 12211, USA

§ Current address: Washington & Jefferson College, Washington, PA 15301, USA

¶ Current address: MIT, Cambridge, MA 02139, USA

- [1] N. Isgur and G. Karl, Phys. Rev. **D 18**, 4187 (1978); S. Capstick and N. Isgur, Phys. Rev. **D 34**, 2809 (1986); S. Capstick and W. Roberts, Prog. Part. Nucl. Phys. **45**, S241 (2000).
- [2] E. Oset and A. Ramos, Nucl. Phys. **A635**, 99 (1998); J. A. Oller and U. G. Meissner, Phys. Lett. **B 500**, 263 (2001); T. Hyodo and D. Jido, Prog. Part. Nucl. Phys. **67**, 55 (2012); Y. Ikeda, T. Hyodo, and W. Weise, Nucl. Phys. **A881**, 98 (2012).
- [3] Y. Akaishi and T. Yamazaki, Phys. Rev. **C 65**, 044005 (2002); Y. Akaishi, T. Yamazaki, M. Obu, and M. Wada, Nucl. Phys. **A835**, 67 (2010).
- [4] R. J. Hemingway, Nucl. Phys. **B253**, 742 (1985).
- [5] D. W. Thomas *et al.*, Nucl. Phys. **B56**, 15 (1973).
- [6] R. H. Dalitz, Eur. Phys. J. C **3**, 676 (1998).
- [7] O. Kittel and G. R. Farrar, arXiv:hep-ph (2000), arXiv:0010186 [hep-ph]; (2005), arXiv:0508150 [hep-ph].
- [8] A. Engler *et al.*, Phys. Rev. Lett. **15**, 224 (1965).
- [9] K. Moriya *et al.* (CLAS Collaboration), Phys. Rev. C **87**, 035206 (2013).
- [10] K. Moriya *et al.* (CLAS Collaboration), Phys. Rev. C **88**, 045201 (2013).
- [11] R. A. Schumacher and K. Moriya, Nucl. Phys. **A914**, 51 (2013).
- [12] N. Byers and S. Fenster, Phys. Rev. Lett. **11**, 52 (1963).
- [13] K. Moriya, Ph.D. thesis, Carnegie Mellon University, (2010), available online at http://www.jlab.org/Hall-B/general/clas_thesis.html.

W (GeV)	$\cos \theta_{K^+}^{\text{c.m.}}$	Q_x	Q_y	$Q_z = \vec{P} $
2.55–2.65	0.60–0.70	-0.06 ± 0.06	-0.02 ± 0.06	0.38 ± 0.05
2.55–2.65	0.70–0.80	-0.04 ± 0.05	0.01 ± 0.05	0.43 ± 0.05
2.55–2.65	0.80–0.88	-0.09 ± 0.07	0.06 ± 0.07	0.47 ± 0.06
2.65–2.75	0.60–0.70	-0.09 ± 0.07	-0.11 ± 0.06	0.36 ± 0.07
2.65–2.75	0.70–0.80	0.03 ± 0.06	0.08 ± 0.06	0.59 ± 0.06
2.65–2.75	0.80–0.86	0.14 ± 0.09	-0.01 ± 0.09	0.38 ± 0.08
2.75–2.85	0.60–0.70	0.05 ± 0.08	-0.11 ± 0.08	0.40 ± 0.08
2.75–2.85	0.70–0.80	-0.02 ± 0.07	0.08 ± 0.07	0.55 ± 0.06
2.75–2.85	0.80–0.86	-0.05 ± 0.09	-0.13 ± 0.10	0.48 ± 0.09
Full range	Full range	-0.03 ± 0.02	0.00 ± 0.02	0.45 ± 0.02

TABLE I. Measured Σ^+ polarization components with statistical uncertainties in the x , y , and z directions for each kinematic bin. The z direction is the out-of-plane production and polarization direction. The y direction is the initial-state proton axis, and the x direction is $\hat{y} \times \hat{z}$.